Journal of Power Sources 198 (2012) 383–388

Contents lists available at SciVerse ScienceDirect

Journal of Power Sources

journal homepage: www.elsevier.com/locate/jpowsour

# Electrochemical hydrogen storage performance of $Mg_{2-x}Al_xNi$ thin films

Junli Xu*, Dun Niu, Youjing Fan

*College of Science, Northeastern University, Shenyang 110004, China*

ARTICLE INFO

*Article history:*
Received 20 April 2011
Received in revised form 4 September 2011
Accepted 21 September 2011
Available online 29 September 2011

*Keywords:*
Hydrogen storage alloy
$Mg_2Ni$ thin film
Al substitution
Charge–discharge property

ABSTRACT

$Mg_{2-x}Al_xNi$ thin films ($x = 0$, 0.1, 0.2, 0.3) are prepared by magnetron sputtering. Their charge–discharge properties are tested, and the effects of Al partial substitution for Mg on the change of the enthalpy of hydrides formation and electrochemical properties are discussed. The charge–discharge experiments show that the discharge properties of the $Mg_2Ni$ film are improved by the substitution of Al for Mg. The change of the enthalpy of hydrides formation of the $Mg_{2-x}Al_xNi$ film decrease with the increase of Al content, which indicate that the stability of the $Mg_{2-x}Al_xNi$ film hydrides decrease with the increase of Al content. The potentiodynamic polarization results show that the anti-corrosion property of $Mg_2Ni$ thin film is improved with the partial substitution of Al for Mg. Electrochemical impedance spectra studies suggest that the oxide layer thickness decrease with Al substitution, and the charge-transfer resistance of the film electrode increase from 202 Ω ($Mg_2Ni$) to 1474 Ω ($Mg_{1.6}Al_{0.4}Ni$) which indicates that the reaction rate at the electrode surface decrease.



## 1. Introduction

Mg-base hydrogen storage alloys are more promising materials for Ni-metal hydride rechargeable batteries than $AB_5$- and $AB_2$-type alloys because of their high theoretical capacities and lower cost for hydrogen absorption/desorption [1–5]. Nowadays, Mg-based thin films for hydrogen storage have attracted a lot of attention yielding several remarkable results. Sapru et al. [6] and Ovhinsky et al. [7,8] reported in their patents that MgNi-based thin film electrodes exhibited an energy density of more than 500 mAh $g^{-1}$ at a discharge current of 50 mA $g^{-1}$. Higuchi et al. [9] and Yoshimura et al. [10] mentioned that the desorption temperature from the magnesium hydride is lower than 373 K in the Pd–Mg film. Richardson et al. [11] demonstrated that Pd-capped Mg–Ni thin films readily react with hydrogen at room temperature (RT) and low pressure (<100 Pa). Ouyang et al. [12] suggested that the hydrogen absorption content reached 4.6 mass% at room temperature and hydrogen desorption reached 3.4 mass% hydrogen. Domènech-Ferrer et al. [13] found that the nanostructured Mg films could be hydrogenated at temperature as low as 50 C in a few minutes. Niessen and Notten [14] observed that the maximum reversible hydrogen storage capacity at the optimal composition ($Mg_{80}Sc_{20}$) amounts to 1795 mAh $g^{-1}$ corresponding to a hydrogen content of 2.05 hydrogen atoms per metal or 6.7 mass%, which is close to five times that of the commonly used hydride-forming materials in commercial Ni–MH batteries. Nevertheless, these thin films showed poor cycling stability, and the discharge capacities decay seriously with increase in the number of cycles.

It has been shown that Al is an effective additive to improve the capacity and the cycle life of Mg–Ni based bulk alloys [15–20]. Most of them suggested that the improved cyclic lifetimes with Al substitution for $Mg_2Ni$ type electrodes is due to the formation of $Al_2O_3$ on the surface of the alloy which prevents the alloy from being further oxidized. This however is contrary to observations of Sakai et al. [21], who found that Al easily dissolved in 6 M KOH in which case there would be no $Al_2O_3$ formation. Sato et al. [22] pointed out that Al-doping of $Mg_2NiH_4$ was counteracted by cycling and only had a temporary influence on the properties.

In the present work, $Mg_{2-x}Al_xNi$ thin films were prepared using magnetron sputtering, and the charge/discharge characteristics of these alloys were investigated, and the effects of the partial substitution of Mg with Al on the electrode properties were discussed systematically.

## 2. Experimental methods

$Mg_{2-x}Al_xNi$ ($x = 0$, 0.2, 0.3, 0.4) thin films were prepared by DC magnetron sputtering. The details of the sputtering conditions were described in a previous paper [23]. The charge/discharge electrochemical properties were tested in a half-cell consisting of the MH working electrode, the $NiOOH/Ni(OH)_2$ counter electrode and 6 M KOH electrolyte. The electrodes were charged at a current density of 1 mA $cm^{-2}$ for 1 h, rested for 1 min, and then discharged at 0.01 mA $cm^{-2}$. The cut-off voltage for the charge and discharge processes was 1.5 V and 0.9 V (vs. NiOOH) separately.

* Corresponding author. Tel.: +86 24 83684533; fax: +86 24 83684533.
*E-mail address:* jlxu@mail.neu.edu.cn (J. Xu).

0378-7753/$ – see front matter © 2011 Elsevier B.V. All rights reserved.
doi:10.1016/j.jpowsour.2011.09.059

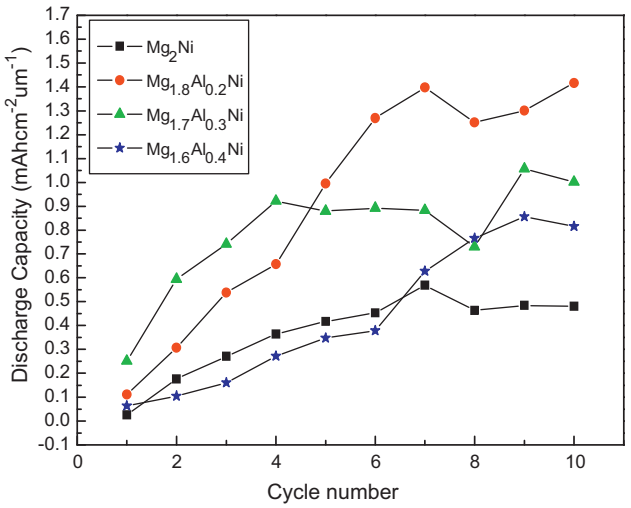


**Fig. 1.** Effect of cycle number on discharge capacities of $Mg_{2-x}Al_xNi$ film electrodes.

Electrochemical tests were performed at 298 K in 6 M KOH solution with a three-electrode cell using EGG Princeton Applied Research (PAR) 2273. The counter electrode was a Pt plate and the reference electrode was an Hg/HgO electrode.

For pressure-composition isotherms (PCT curves) at different temperature measurement, the alloy electrodes were first charged at a current density of 1 mA $cm^{-2}$ for 1 h. The electrodes were discharged at a current density of 0.25 mA $cm^{-2}$ for 15 min followed by a rest period under open-circuit condition for the potential to become constant, and then the discharge and rest procedure was repeated until the electrodes reached the cut-off potential of −0.6 V vs. Hg/HgO reference electrode.

The potentiodynamic polarization curves were measured at a scanning rate of 0.166 mV $s^{-1}$. The electrochemical impedance spectra (EIS) of the electrodes were obtained in the frequency range from 100 kHz to 10 mHz with an AC amplitude of 5 mV applied to the electrode under the open-circuit condition. For EIS data simulation, the ZSimpWin software was used.

## 3. Results and discussion

### 3.1. Charge–discharge properties

The deposited $Mg_{2-x}Al_xNi$ thin films were characterized as described in the previous paper as follows [23]: The film thickness was about 7 μm with a columnar structure in the deposition direction, and the grain size was less than 30 nm detected by TEM. The compositions of the thin films were $Mg_2Ni$ and $Mg_2Al_3$.

Fig. 1 shows the variation of the discharge capacity of the $Mg_{2-x}Al_xNi$ thin film alloy versus the number of cycles. As shown in Fig. 1, the discharge capacity was improved to some degree with the substitution of Al for Mg. The maximum capacity was achieved in $Mg_{1.8}Al_{0.2}Ni$ with a 1.4 mAh $cm^{-2}$ μ$m^{-1}$ value.

Moreover, it can be observed from Fig. 1 that the capacity increased first with increasing cycle number, then varied further with increasing cycle number. The first increase capacity with increasing cycle number is mainly because of the increase of the active surface with cycle number. At the same time, the oxides formed in the thin film surface with the increasing cycle number, and thus the capacity decreased. With the oxide layers cracked, a new fresh hydrogen storage alloy surface was exposed, and H atom is more easily absorbed into the alloy, which results in the increased capacity again. Fig. 2 shows the surface of $Mg_{1.7}Al_{0.3}Ni$ thin films before and after ten charge–discharge processes. It can be seen from Fig. 2b and c that a discontinuous layer covers the thin film alloys after ten charge–discharge processes which is composed of Mg, Al, Ni, O and K elements identified by EDAX, as shown in Fig. 3. The atom percentage of O element is much higher than K, which implies that the content of oxides is high in the layer.

The results from the electrochemical discharge tests undertaken in this study showed that the discharge capacity of the film increased with Al substitution for Mg. In order to account for these results, it is necessary to investigate the effect of Al substitution for Mg on the electrochemical properties of the $Mg_2Ni$ thin film alloy electrodes. A number of electrochemical tests, namely electrochemical PCT isotherms, polarization and EIS were carried out.

### 3.2. Change of the enthalpy of hydride formation

Metal hydrides are formed by chemical reaction between hydrogen and metal and this is associated with the release of heat ($\Delta H^\theta$, the change of enthalpy of hydride formation) for the stable hydrides. The more thermodynamically stable the hydride is, the larger the absolute value of $\Delta H^\theta$, and the higher temperature is needed in order to desorb hydrogen (reverse reaction). Kleperis et al. [24] stated that if the value of $\Delta H^\theta$ ranges between −25 kJ $mol^{-1}$ and −50 kJ $mol^{-1}$, the alloy is a viable candidate for battery applications.

From Van't Hoff equation, $\ln p(H_2) = \Delta H^\theta/RT - \Delta S^\theta/R$, we can induce that there is a linear correlation between $\ln p(H_2)$ and $1/T$, and the slope is $\Delta H^\theta/R$. Here, $p(H_2)$ [atm] is the equilibrium hydrogen pressure, $R$ is the universal gas constant, $T$ is the temperature, $\Delta H^\theta$ is the change of enthalpy, and $\Delta S^\theta$ is the change of entropy of the hydride formation.

From the Nernst equation, we can know that the electrode equilibrium potential ($E_{eq}$) measured in solution is linked to the hydrogen equilibrium pressure measured in gas phase. By detecting the electrode equilibrium potential at different capacity, we can calculate the related hydrogen equilibrium pressure using the Nernst equation. Thus, we can obtain the dependence of the equilibrium pressure versus the amount of absorbed or desorbed hydrogen known also as the electrochemical PCT isotherm [25]. On the basis of the Nernst equation, the relationships of the $E_{eq}$ value of the MH electrode in alkaline solution (measured with respect to the Hg, $HgO/OH^-$ reference electrode) with the equilibrium pressure of hydrogen is as follows [26]:

$$E_{eq} = E^\theta(H_2O/H_2) - E^\theta(Hg, HgO/OH^-) - (RT/2F)\ln\{[\alpha(H_2O)/\gamma(H_2)][p(H_2)/p^\theta]\} \quad (1)$$

Where $E^\theta(H_2O/H_2)$ and $E^\theta(Hg, HgO/OH^-)$ are the standard potentials of the $H_2O/H_2$ couple and Hg, $HgO/OH^-$ redox couples respectively; $\alpha(H_2O)$ is the activity of water, $\gamma(H_2)$ is the fugacity coefficient of hydrogen, and $p^\theta$ is the standard pressure. According to Ref. [27], the relationships between the $E_{eq}$ and $P_{H_2}$ at 298 K, 303 K, 308 K in 6 M KOH solution at 1atm pressure are calculated as follows:

$$298\,K,\quad E_{eq} = -0.9205 - 0.01284\ln p(H_2)(V\text{vs.Hg/HgO}) \quad (2a)$$

$$303\,K,\quad E_{eq} = -0.9191 - 0.01305\ln p(H_2)(V\text{vs.Hg/HgO}) \quad (2b)$$

$$308\,K,\quad E_{eq} = -0.9177 - 0.01327\ln p(H_2)(V\text{vs.Hg/HgO}) \quad (2c)$$

The electrochemical PCT curves for hydrogen desorption of $Mg_{2-x}Al_xNi$ hydrides at different temperatures are shown in Fig. 4. It can be seen that the increase of temperature results in an increase of the plateau pressure, and the partial substitution of Al for Mg results in an increase of the plateau pressure of the hydride. The pressure increase with Al addition is related to the decrease of interatomic distances and from the lower affinity of element of Al with hydrogen [28]. However, the plateau pressure was not obvious for

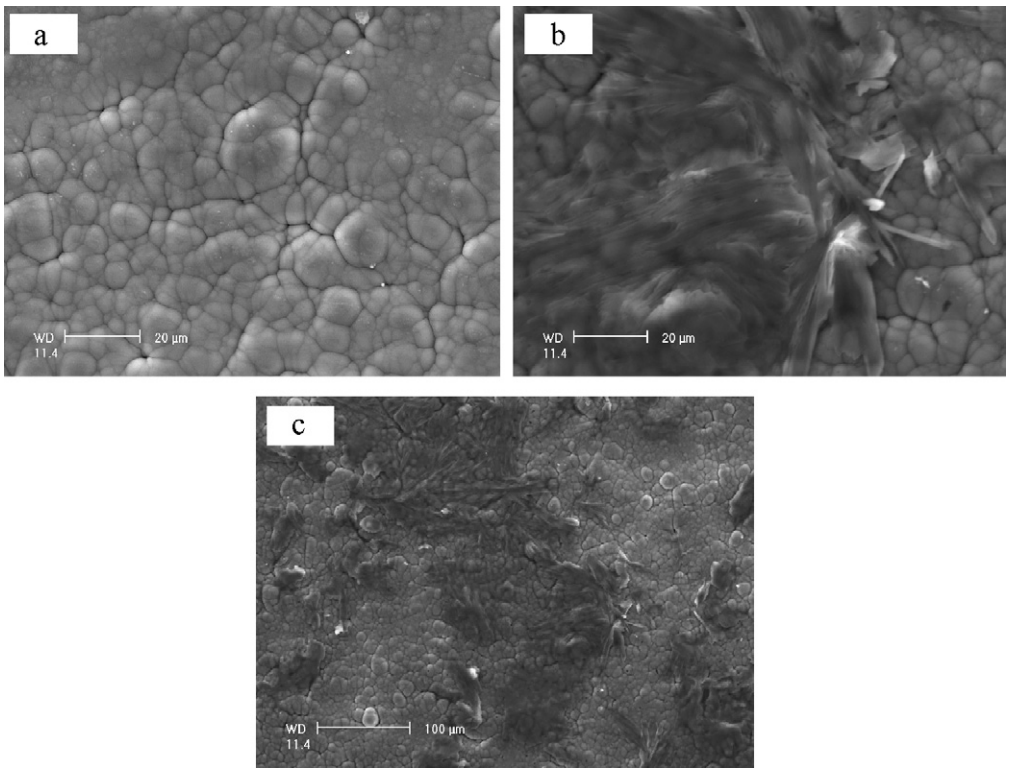


**Fig. 2.** SEM images of the surface of $Mg_{1.7}Al_{0.3}Ni$ thin films. (a) before charge–discharge processes and (b), (c) after 10 charge–discharge processes.

**Table 1**
The change enthalpy of $Mg_{2-x}Al_xNi$ thin film hydrides formation.

| Alloys | The change in standard enthalpy ($kJ\,mol^{-1}$) |
|---|---|
| $Mg_2Ni$ | −34.18 |
| $Mg_{1.8}Al_{0.2}Ni$ | −24.18 |
| $Mg_{1.7}Al_{0.3}Ni$ | −24.83 |
| $Mg_{1.6}Al_{0.4}Ni$ | −22.79 |

all the thin film alloys. This is mainly because the components of the thin film alloys were not well distributed [29].

Fig. 5 shows the relationship between the plateau pressures of their hydrides with the temperature. The change of enthalpy of $Mg_{2-x}Al_xNi$ thin film hydrides was obtained by a linear fit, as shown in Table 1.

It can be seen from Table 1 that the change of enthalpy of formation $Mg_2Ni$ thin film hydrides is about $-34\,kJ\,mol^{-1}$. The absolute value is less than $65\,kJ\,mol^{-1}$, which is the absolute value of the change of enthalpy of $Mg_2Ni$ alloy hydride formation [30]. Moreover, the absolute of change of enthalpy of $Mg_{2-x}Al_xNi$ thin film hydrides formation decreased with the substitution of Al for Mg, which suggests that the thermal stability of $Mg_2Ni$ thin film hydrides is lowered with substitution of Al for Mg. Thus, the H atom was easier to be released from the hydrides with Al substitution for Mg.

### 3.3. Polarization analysis

Since the corrosion of Mg-based alloys is a barrier to its practical use, we investigated the corrosion behavior of $Mg_{2-x}Al_xNi$ thin film alloys in 6 M KOH solution.

Typical potentiodynamic polarization curves obtained for the $Mg_{2-x}Al_xNi$ ($x = 0$, 0.2, 0.3, 0.4) thin films in 6 M KOH solution are shown in Fig. 6. It is observed that the corrosion potential of the thin films increases, and the passive current becomes smaller with the Al partially substituted for Mg. This suggests that the anodic process is inhibited, and the anti-corrosion behavior is improved to a certain degree with the addition of Al.

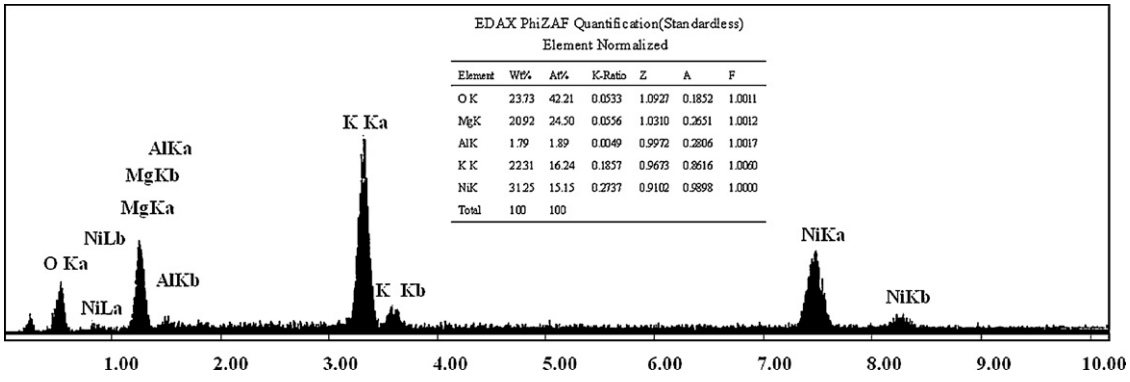


**Fig. 3.** The EDAX analysis results for the map of Fig. 2b.

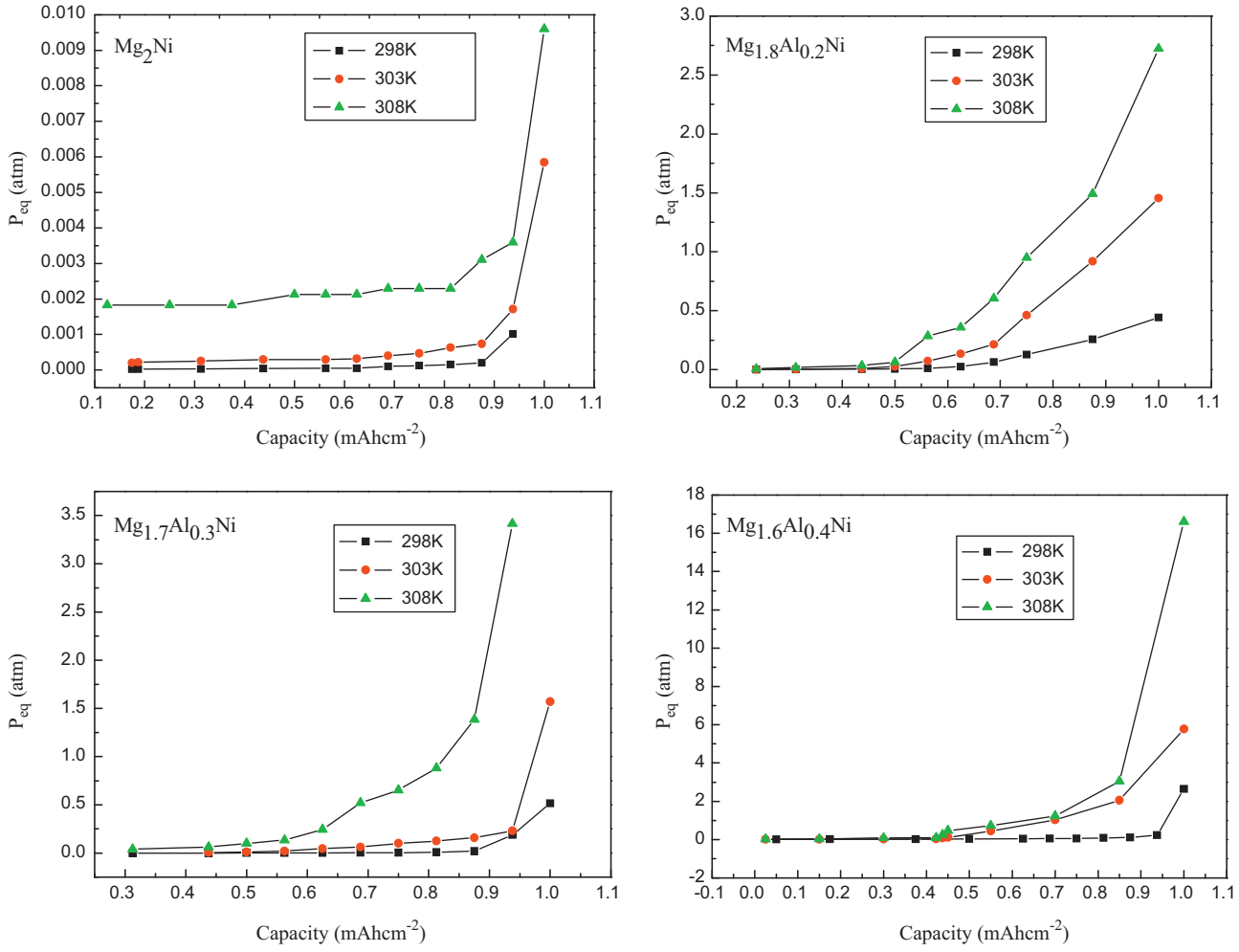


**Fig. 4.** Electrochemical discharging isotherms at different temperature of $Mg_{2-x}Al_xNi$ thin film hydrides.

### 3.4. Electrochemical impedance spectra analysis

Fig. 7 shows the EIS Nyquist plots of the $Mg_{2-x}Al_xNi$ ($x$ = 0, 0.2, 0.3, 0.4) thin film electrodes at open potential in 6 M KOH solution at 298 K. It can be seen that the Nyquist plots for the electrodes ($x$ = 0, 0.2, 0.3) consists of two obvious capacitive loops, while the plot for the thin film electrode ($x$ = 0.4) has only one. One of the capacitive loops may be attributed to corrosion product formation at the surface of the film. When the corrosion product forming at the electrode surface is thick enough, the corrosion product deposit properties will be reflected in the EIS spectra.

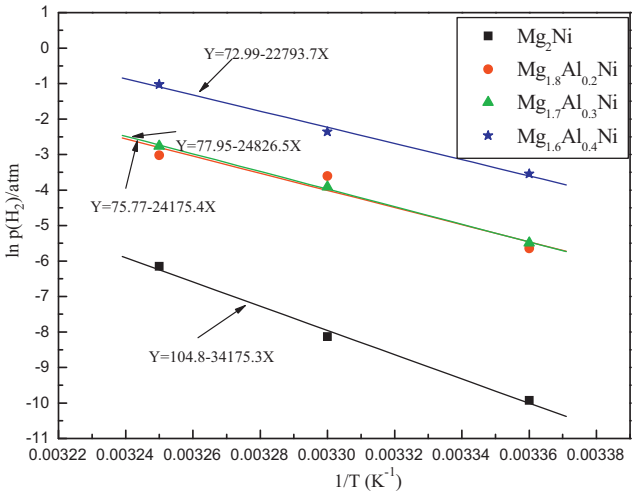


**Fig. 5.** The van't Hoff plots for the $Mg_{2-x}Al_xNi$–$H_2$ system, obtained using the data from Fig. 4.

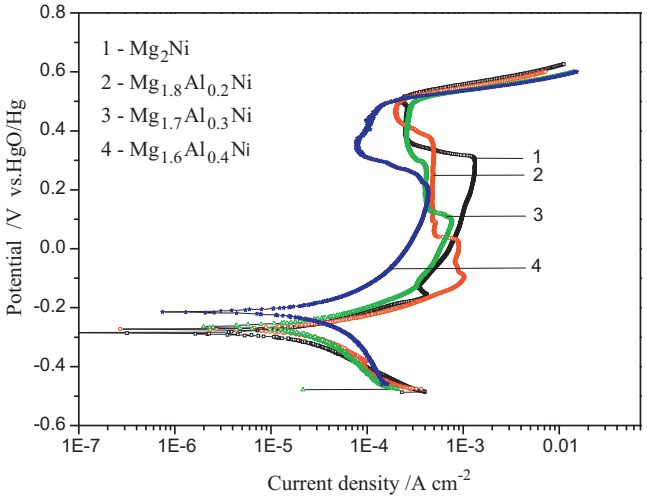


**Fig. 6.** Potentiodynamic polarization plots of the thin film electrodes in 6 M KOH solution with a scan rate of 0.166 mV $s^{-1}$ at 298 K.

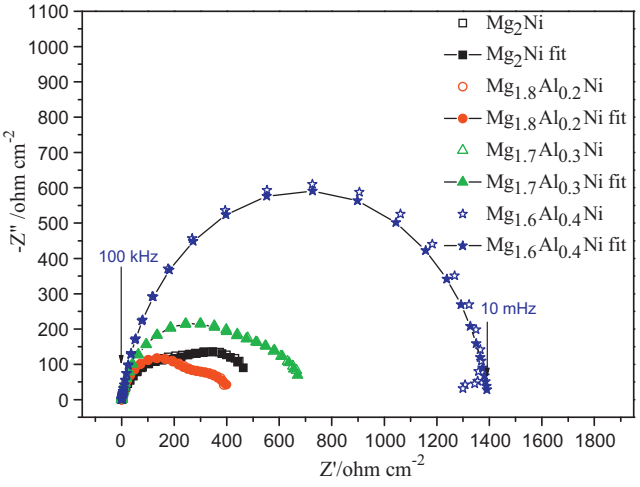


**Fig. 7.** Electrochemical impedance spectra of the thin film electrodes measured at the open-circuit at 298 K, compared with model fit.

To verify the above inference, EIS responses of the $Mg_2Ni$ thin film electrode at different temperatures were carried out, and the results are given in Fig. 8. We can see that the Nyquist plots for the thin film electrodes at the low temperatures only consisted of one capacitive loop. As the temperature is increased, another capacitive loop is observed. Furthermore, with increasing temperature, the radius of the arc at the low-frequency region is increased, while that at the high-frequency region is decreased. This implies that the capacitive loop at low frequencies is a characteristic of the charge transfer process at the alloy/electrolyte interface since reaction rate accelerate with increasing temperature. The capacitance at the high-frequency region is attributable to the formation of corrosion products at the surface of film.

Two equivalent circuit models for the frequency response of the electrodes are given in Fig. 9. Considering the porosity and roughness of the electrode surface, constant-phase elements (CPE) are used in this circuit model. In this circuit, $R_s$ is the electrolyte resistance between the film electrode and the reference electrode, $Q_{dl}$ is the double layer capacitance and $R_{ct}$ is the charge-transfer resistance. The capacitance ($Q_o$) parallel to an electronically insulating resistance ($R_o$) accounts for the formation of corrosion products at the electrode surface.

The models fitted to the experimental data as illustrated in Fig. 7 show good agreement. Parameter values of this model were

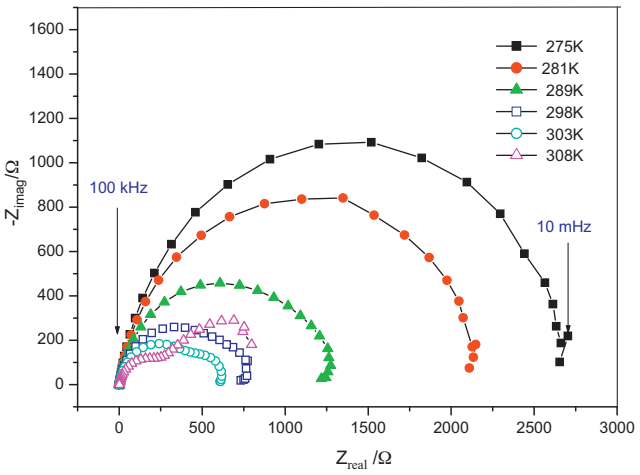


**Fig. 8.** Nyquist plot for $Mg_2Ni$ film electrode at various temperatures at the open-circuit.

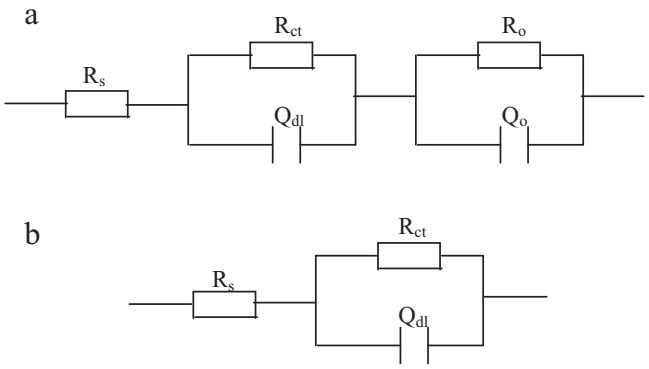


**Fig. 9.** Equivalent circuit models representing the electrode/electrolyte face: (a) for two capacitance and (b) for one capacitance.

obtained by fitting of the plots with ZSimpWin software, and the results are listed in Table 2. The charge-transfer resistance $R_{ct}$ of the film electrode increased from 202 Ω ($Mg_2Ni$) to 1474 Ω ($Mg_{1.6}Al_{0.4}Ni$) which indicates that the reaction rate at the electrode surface decreased with Al partial substitution. As insulating resistance ($R_o$) values characterize the corrosion product layer thickness, we can conclude that the corrosion product layer thickness at the electrode surface decreased with Al addition.

For $Mg_{2-x}Al_xNi$ alloy, there are some possible reactions in the KOH electrolyte as follows:

$$H_2 + 2OH^- = 2H_2O + 2e^- \varphi^\theta = -0.828\,V \quad (3a)$$

$$Mg + 2OH^- = Mg(OH)_2 + 2e^- \varphi^\theta = -2.68\,V \quad (3b)$$

$$Ni + 2OH^- = Ni(OH)_2 + 2e^- \varphi^\theta = -0.69\,V \quad (3c)$$

$$Al + 4OH^- = Al(OH)_4^- + 3e^- \varphi^\theta = -2.31\,V \quad (3d)$$

From the above equations, it is obvious that Mg and Al are easily corroded in the alkaline electrolyte forming $Mg(OH)_2$ and $Al(OH)_4^-$. For the $Mg_2Ni$ film, only $Mg(OH)_2$ formed in the KOH solution during discharge progress. Gulbrandsen et al. [31] and Nordlien et al. [32] pointed out that the $Mg(OH)_2$ passive film is porous and permeable to KOH and thus cannot protect the inner fresh surface from corrosion. Since $Mg(OH)_2$ solubility product is high, $Mg^{2+}$ ions exist in the solution. With Al partial substitution for Mg, $Al(OH)_3$ may be formed because of double hydrolyze reactions as Eq. (4) shows.

$$Mg^{2+} + 2Al(OH)_4^- = Mg(OH)_2 + 2Al(OH)_3 \quad (4)$$

The $Al(OH)_3$ solubility is much smaller than $Mg(OH)_2$, so the $Al(OH)_3$ layer is more compact and hence the penetration of $OH^-$ ion through the oxide layer is more difficult, offering greater and more effective protection to the inner fresh alloy. As a result, the anti-corrosion properties of the film are enhanced with Al addition.

Moreover, with Al dissolving in Mg crystal lattice, the volume changes will decrease upon cycling. This is also good for anti-pulverization, which will increase the discharge capacity. Also, small volume changes can decrease the possibility of transport of easily oxidized alloy components to the electrode surface [33].

In addition to inhibiting $OH^-$ penetration, the oxide layer on the alloy surface may also act as a barrier for hydrogen diffusion into and out of the alloy during the charge–discharge cycling in alkaline solution which is undesirable. In order to generate a practicable thin surface layer, both effects must essentially come to a compromise. If the Al content in the alloy is too low, the oxide layer on the electrode surface is too porous, and shows weak anticorrosive ability. On the other hand, if the Al content in the alloy is too high, the oxide layer will be too dense, and in addition to blocking $OH^-$ penetration, also retards the hydrogen diffusion and the charge transfer

**Table 2**
Equivalent circuit parameters in 6 M KOH solutions at the potential of 0 V.

| Sample | $R_s$ (Ω) | $Q_{dl}$ (F cm$^2$) | $R_{ct}$ (Ω) | $\alpha_1$ | $Q_o$ (F cm$^2$) | $R_o$ (Ω) | $\alpha_2$ |
|---|---|---|---|---|---|---|---|
| $Mg_2Ni$ | 0.305 | 2.336E−4 | 202 | 0.827 | 1.686E−3 | 322 | 0.806 |
| $Mg_{1.8}Al_{0.2}Ni$ | 0.496 | 2.134E−4 | 208 | 0.943 | 3.99E−3 | 226 | 0.663 |
| $Mg_{1.7}Al_{0.3}Ni$ | 0.449 | 2.300E−4 | 435 | 0.892 | 3.417E−3 | 267 | 0.846 |
| $Mg_{1.6}Al_{0.4}Ni$ | 0.339 | 2.114E−4 | 1474 | 0.847 | | | |

reaction on the surface of the films. The suitable formation of passive films should offer good corrosion protection as well as allowing for the diffusion of H atom, which determines the electrochemical property of the electrode. The results obtained in this study indicate that the $Mg_{1.7}Al_{0.2}Ni$ thin film exhibits outstanding discharge performance.

## 4. Conclusions

The discharge property of $Mg_2Ni$ film was improved by the substitution of Al for Mg. As the Al content increased, the stability of the $Mg_{2-x}Al_xNi$ hydrides decreased. The anti-corrosion property of $Mg_{2-x}Al_xNi$ alloy was enhanced with the addition of Al since $Al(OH)_3$ oxide layer may be formed, which can more effectively inhibit $OH^-$ penetration to the inner of the alloy electrode. However, the charge-transfer resistance of the film electrode increased with Al partial substitution for Mg, which indicates that the reaction rate at the electrode surface is decreased. There exists a best value of the Al content for the $Mg_{2-x}Al_xNi$ thin film electrode properties. In this study, $Mg_{1.7}Al_{0.2}Ni$ shows the highest discharge capacity.

## Acknowledgements

The authors would like to acknowledge Prof. Geir Martin Haarberg of the Norwegian University of Science and Technology for kindly improving the English of this paper, and the financial support from the National Natural Science Foundation of China (No. 51104042).

## References

[1] P.I. Jain, C. Lal, A. Jain, Int. J. Hydrogen Energy 35 (2010) 5133–5144.
[2] D. Mu, Y. Hatano, T. Abe, K. Watanabe, J. Alloys Compd. 334 (2002) 232–237.
[3] R. Vijay, R. Sundaresan, M.P. Maiya, S. Srinivasa Murthy, Int. J. Hydrogen Energy 30 (2005) 501–508.
[4] X. Liu, Y. Zhu, L. Li, Int. J. Hydrogen Energy 32 (2007) 2450–2454.
[5] Y. Ikeda, T. Ohmori, Int. J. Hydrogen Energy 34 (2009) 5439–5443.
[6] K. Sapru, B. Reichman, A. Reger, S.R. Ovshinsky, Rechargeable battery and electrode used therein, US patent no. 4623, 597, Nov.18, 1986.
[7] S.R. Ovshinsky, M.A. Fetcenko, Electrochemical hydrogen storage alloys and batteries fabricated from Mg containing base alloys, US patent no. 5,506,069, April 9, 1996.
[8] S.R. Ovshinsky, M.A. Fetcenko, J. Im, B. Chao, B. Reichman, K. Young, Electrochemical hydrogen storage alloys and batteries containing heterogeneous powder particles, US patent no. 5,554,456, September 10, 1996.
[9] K. Higuchi, K. Yamamoto, H. Kajioka, K. Toiyama, M. Honda, S. Orimo, H. Fujii, J. Alloys Compd. 330–332 (2002) 526–530.
[10] K. Yoshimura, Y. Yamade, M. Okada, Surf. Sci. 566–568 (2004) 751–754.
[11] T.J. Richardson, J.L. Slack, R.D. Armitage, R. Kostecki, B. Farangis, M.D. Rubin, Appl. Phys. Lett. 78 (2001) 3047–3049.
[12] L.Z. Ouyang, H. Wang, C.Y. Chung, J.H. Ahn, M. Zhu, J. Alloys Compd. 422 (2006) 58–61.
[13] R. Domènech-Ferrer, M.G. Sridharan, G. Garcia, F. Pi, J. Rodríguez-Viejo, J. Power Sources 169 (2007) 117–122.
[14] R.A.H. Niessen, P.H.L. Notten, J. Alloys Compd. 404–406 (2005) 457–460.
[15] J. Xue, G. Li, Y. Hu, J. Alloys Compd. 307 (2000) 240–244.
[16] H.T. Yuan, L.B. Wang, R. Cao, Y.J. Wang, Y.S. Zhang, D.Y. Yan, W.H. Zhang, W.L. Gong, J. Alloys Compd. 309 (2000) 208–211.
[17] H. Yuan, Q. Li, H. Song, Y. Wang, J. Liu, J. Alloys Compd. 353 (2003) 322–326.
[18] L. Smardz, M. Jurczyk, K. Smardz, M. Nowak, M. Makowiecka, I. Okonska, Renew. Energy 33 (2008) 201–210.
[19] J. Guo, R. Zhang, W.Q. Jiang, G.X. Li, W.L. Wei, J. Alloys Compd. 429 (2007) 348–351.
[20] A. Gasiorowski, W. Iwasieczko, D. Skoryna, H. Drulis, M. Jurczyk, J. Alloys Compd. 364 (2004) 283–288.
[21] T. Sakai, H. Yoshinaga, H. Miyamura, N. Kuriyama, H. Ishikawa, J. Alloys Compd. 180 (1992) 37–54.
[22] T. Sato, H. Blomqvist, D. Noreus, J. Alloys Compd. 356–357 (2003) 494–496.
[23] J. Xu, Y. Li, F. Wang, Electrochim. Acta 55 (2009) 148–154.
[24] J. Kleperis, G. Wojcik, A. Czerwinski, J. Skowronski, M. Kopczyk, M. Beltowska-Brzenska, J Solid State Electrochem. 5 (2001) 229–249.
[25] S. Bliznakov, E. Lefterova, N. Dimitrov, Int. J Hydrogen Energy 33 (2008) 5789–5794.
[26] J. Kleperis, G. Wojcik, A. Czerwinski, J. Skowronski, M. Kopczyk, M. Beltowska-Brzezinska, J. Solid State Electrochem. 5 (2001) 229–249.
[27] J. Balej, Int. J. Hydrogen Energy 10 (1985) 365–374.
[28] S. Orimo, K. Ikeda, H. Fujii, S. Saruki, T. Fukunaga, A. Zuttel, L. Schlapbach, Acta Mater. 46 (1998) 4519–4525.
[29] K.H. Buschow, H.H. Van Mal, H.H. Van Mal, J. Less-Common Met. 29 (1973) 203–210.
[30] K. Zeng, T. Klassen, W. Oelerich, R. Bormann, J. Alloys Compd. 283 (1999) 213–224.
[31] E. Gulbrandsen, J. Tafto, A. Olsen, Corros. Sci. 34 (1993) 1423–1440.
[32] J.H. Nordlien, S. Ono, N. Masuko, K. Nisancioglu, J. Electrochem. Soc. 142 (1995) 3320–3322.
[33] J.J.G. Willems, K.H.J. Buschow, J. Less-Common Met. 129 (1987) 13–30.